Article

Physical-Mechanical Properties of Chartwell® Coupling Agent-Treated Calcium Carbonate and Silica-Reinforced Hybrid Natural Rubber Composites

Gabriel Deltrejo Ribeiro [1], Carlos Toshiyuki Hiranobe [1], José Francisco Resende da Silva [1], Giovanni Barrera Torres [2], Leonardo Lataro Paim [1], Aldo Eloizo Job [3], Flávio Camargo Cabrera [1] and Renivaldo José dos Santos [1,*]

[1] Departamento de Engenharia de Energia, Faculdade de Engenharia e Ciências, Campus de Rosana, Universidade Estadual Paulista (UNESP), Avenida dos Barrageiros, Rosana 19274-000, SP, Brazil

[2] Departamento de Ingeniería de Diseño Industrial, Instituto Tecnológico Metropolitano (ITM), Medellín, Antioquia 050036, Colombia

[3] Departamento de Física, Faculdade de Ciência e Tecnologia, Campus de Presidente Prudente, Universidade Estadual Paulista (UNESP), Rua Roberto Simonsen, Presidente Prudente 19060-900, SP, Brazil

* Correspondence: renivaldo.santos@unesp.br

Abstract: In this work investigated the possibility of applying a superficial treatment to ultra-fine calcium carbonate aiming to improve its interaction with the polymer chains of natural rubber so it does not act just as a filler. Commercial processes commonly use 40 phr of Silica as reinforcement filler. Here, we have evaluated the partial replacement of Silica by two types of calcium carbonate into hybrid natural rubber composites, untreated ultra-fine calcium carbonate and with ultra-fine calcium carbonate treated with 2% Chartwell C-515.71HR®. We added calcium carbonate fillers to the composite mixtures (as replacements for commercial silica treated with silane) and studied their influence on the vulcanization process. According to our findings, between 25% and 75% of the silica can be replaced with treated calcium carbonate, and up to 30 parts of $CaCO_3$ can be combined with 100 parts of NR without compromising the properties of the polymer matrix (NR), which generates economic advantages for this industry. Treated calcium carbonate was able to link the inorganic and organic parts of the composite due to its bifunctionality; hence, it can be used as a filler to partially replace silica in hybrid NR composites.

Keywords: NR-$CaCO_3$ composites; vulcanization; crosslink density; mechanical properties; coupling agent

1. Introduction

Natural rubber (cis-1,4-polyisoprene) is one of the most valuable renewable elastomers due to its excellent physical-mechanical properties, such as high tensile strength, flexibility, and elasticity. It is amazingly versatile in all its applications, tremendously varied, and comes in the form of latex or coagulated and vulcanized. As a result, it is present in the most diverse sectors, e.g., electronic devices with energy storage [1], strain sensors [2], and gas barriers [3]. It is also present in the field of biomaterials, specifically in bone grafting [4], tissue regeneration [5], Nanocomposite as Human-Tissue-Mimicking Materials [6], antibacterial applications [7], and biodegradable films [8]. Additionally, it can be found in the field of engineering in modified asphalt [9], seismic applications [10], and modified cement mortar [11]. In short, Natural Rubber (NR) has great technological potential.

Rubber composites with a high crosslinking density are essential to obtain new mechanical, thermal, and electrical properties in NR. These properties are not achieved by using just curing agents but also fillers widely employed in industrial processes, such as carbon black [12] and silica [13]. In the case of silica, new synthesis methods [14] even from

organic residues such as waste bagasse bottom ash and rice rusk ash [15,16] or preparation of composites with multiwalled carbon nanotubes (MWCNTs) [17] represent an important way to improve its application.

Currently, new fillers are being tested to validate their strengthening potential and find new properties. Among the fillers studied in the literature, we can highlight clay (montmorillonite) [18], halloysite nanotubes [19], graphene nanocomposites [20], sisal and palm oil [21], jute [22], coconut [23], shell powder [24], sugarcane bagasse ash [25], foundry waste [26], and leather waste [27,28]. But why limit us to just one kind of filler? Hybrid composites are combinations of two or more fillers that can provide the new materials with their properties, increasing their interaction possibilities and diversifying their results. Some examples of hybrid composites are pineapple leaf fibers and carbon black [29], bamboo and silica [30], carnauba wax and carbon nanotubes [31], and nanosilica and carbon nanotubes [32].

The problem is that many of these fillers are costly, and others still require expensive and complex surface treatments. In addition, sometimes they need unfeasible processing. For example, silica, which provides one of the greatest mechanical reinforcements among white fillers, is highly expensive, hinders the processing of composites, and requires complementary additives such as polyethylene glycol (PEG), which is widely used as a dispersing agent [33].

Calcium carbonate ($CaCO_3$) is widely used in research to develop NR composites. Lei Jong et al. [34] investigated the synergistic effect between calcium carbonate and soy protein nanoparticles in relation to the tensile properties and low rolling resistance of NR. In another study, Phuhiangpa et al. [35] observed the physical and mechanical properties of rubber composites with $CaCO_3$ powder and demonstrated the possibility of adjusting the mechanical properties of rubber [36]. The effect of the specific surface area of nanocarbonate on the properties of rubber composites was more pronounced in pure natural rubber than in rubber composites filled with calcium microcarbonate.

Sarawut Prasertsri et al. [37] developed hybrid NR composites reinforced with calcium carbonate and carbon black, with calcium carbonate and silica used in different proportions. They showed that the hybrid system of calcium carbonate and carbon black exhibited greater reinforcement efficiency than that of calcium carbonate and silica. In another study, El Mogy et al. [38] investigated the application of biological waste materials (such as eggshells and fishbone) as new fillers in natural rubber composites compared to commercial calcium carbonate. Said fillers presented higher tensile values, modulus at 100% and 300% of elongation, hardness, and abrasion resistance.

Nuchnapa Tangboriboon et al. [39] produced calcium bicarbonate from raw eggshells and applied it to natural rubber latex to make films. They reported good physical-mechanical properties and low protein content due to the raw eggshell powder added to the composites as biofiller.

The size of calcium carbonate particles can be reduced to improve the performance of the composite and increase the interaction between the filler and the polymer matrix; thus, these particles assume the role of a semi-reinforcement filler. However, the interaction between calcium carbonate and natural rubber can also be improved by applying surface treatments with coupling agents such as aluminate [40], zirconate [41], titanate [42], and silane [43].

Chartwell C-515.71HR®, a new coupling agent produced by Chartwell International, Inc., is an organic metal coupling agent with enhanced amino reactant functionality because it is synthesized like a stable neutralized metal complex. It is used similarly to silane [44], i.e., as adhesive and coating on metals, plastics, concrete, elastomers, wood, and ceramics.

In this study, we developed natural rubber composites with ultra-fine calcium carbonate treated with 2% of Chartwell C-515.71HR® as a partial substitute for commercial silica treated with silane and evaluated the influence of this coupling agent as a new option for elastomer vulcanization processes.

2. Experiments

2.1. Materials

This study used Brazilian clear crepe NR (poly-cis-1,4-isoprene) supplied by DLP Indústria e Comércio de Borrachas e Artefatos Ltda, São Paulo, Brazil, with a Mooney viscosity of 84.50 and 0.13% of volatile materials.

Chartwell C-515.71HR® is an organic metal coupling agent with improved amino reagent functionality because it is synthesized like a stable neutralized metal complex. It was supplied as a pale-yellow solution of propylene glycol (solvent) with 7.3–7.9% of metallic content, a specific mass of 1.23 g cm^{-3}, and a pH value of 7.8 in 1% of the solution. Generally, it is used as an adhesive or coating on metals, plastics, concrete, elastomers, wood, and ceramics, and it serves a function similar to that of silane [38]. There is no further available information on Chartwell C-515.71HR® because it is currently under patent protection.

Ultra-fine calcium carbonate (325 mesh) treated with 2% of Chartwell C-515.71HR® and untreated calcium carbonate were supplied ready to use by Aodran do Brasil Comércio de Produtos Químicos Ltda, São Paulo, Brazil.

We acquired amorphous precipitated silica produced by Rhodia Solvay Group (Zeosil® 1165 MP), with a chemical composition of $10SiO_2 \cdot H_2O$ and the appearance of microbeads, due to their high dispersibility and large contact surface. This product is distributed by CYA Rubber Distribuidora Ltd. (Porto Alegre, Brazil) as silane under the trade name Si69® and the chemical name bis (triethoxysilylpropyl) tetrasulfide.

The reagents employed in the composite curing process were purchased commercially and used without prior purification. Additionally, other materials with a high degree of purity were purchased from different suppliers: sulfur from Intercuf Ind. and Com. Ltda, (Campinas, Brazil)., mercaptobenzothiazole disulfide (MTBS) and tetramethylthiuram monosulfide (TMTM) from LANXESS Elastomers do Brasil, stearic acid from Barlocher do Brasil, zinc oxide from Brasoxido, TMQ (2,2,4-trimethyl-1,2-dihydroquinoline) antioxidant from Bayer, and plasticizer oil from Ipiranga Química.

2.2. Preparation of the Composites

The composites were prepared in a Makintec 379M (São José do Rio Preto, Brazil) open cylinder mixer with a friction ratio of 1:1.25 according to ASTM D3182/07 [45]. Due to the difference of one-quarter between the rotation of the cylinders, the shear of the polymer chains occurs and changes the molecular structure to low-viscosity plastic, facilitating the incorporation of fillers and reagents and their reaction with rubber. The masses were measured in phr (per hundred rubber).

The fillers were varied in increments of 10 phr from 40/00 to 00/40 (ultra-fine silica/calcium carbonate), thus reducing the portion of silica treated with silane and increasing that of ultra-fine calcium carbonate treated with Chartwell C-515.71HR® as the coupling agent or that of untreated ultra-fine calcium carbonate. Also, a control sample was produced with the same formulation but without fillers, only pure gum (which means 00/00). Table 1 details the standard vulcanization formulation [28], and Table 2 shows the densities of the composites produced in this study.

First, the NR was plasticized in an open two-roll mixer (Makintec 379M) at approximately 65 °C. After plasticizing the rubber, stearic acid and zinc oxide were added to activate the rubber along with the antioxidant and the plasticizing oil. The fillers were incorporated at the end. In the case of silica, at the time of incorporation, the silane coupling agent (Si69®) was added in a proportion of 5% of the mass of silica used. At the end of the complete homogenization, the samples remained at rest for 24 h, and those with silica rested in an oven at 60 °C (140 °F) to promote silanization.

Accelerators and sulfur were added after the rubber activation period. Remarkably, the crosslinking process was enhanced due to the formation of zinc stearate, a product of the reaction between zinc oxide and stearic acid, which facilitates the action of the accelerators

and the sulfur incorporated later. The function of zinc oxide is to cause the sulfur molecule to break down so that it can promote cross-linking.

Table 1. Standard vulcanization formulation [28].

	Materials and Reagents	Quantity (phr)	Density (g cm^{-3})	Component
1st Stage	Natural Rubber	100	0.95	Polymeric matrix
	Stearic acid	2	0.85	Activator
	Zinc oxide	4	5.57	Activator
	TMQ antioxidant	1	1.20	Additive
	Plasticizing oil	5	0.84	Additive
	Silica (SiO$_2$) + Si69®	40–00	2.10	Filler
	Calcium carbonate (CaCO$_3$)	00–40	2.71	Filler
2nd St.	MBTS [a]	2.5	1.53	Main accelerator
	TMTM [b]	0.5	1.4	Secondary accelerator
	Sulfur	2.5	2.07	Curing agent

[a] MBTS: mercaptobenzothiazole disulfide, [b] TMTM: tetramethyl thiuram monosulfide.

Table 2. Densities of the composites.

Composite (Si/CaCO$_3$)	Density (g cm^{-3})
Gum 00/00	0.99
40/00	1.15
30/10	1.16
20/20	1.17
10/30	1.18
00/40	1.19

Figure 1 presents a summary of the processing of the NR composites studied here. It includes the amount of silica and calcium carbonate in each composite in phr. For instance, the first composite shows a proportion of 40/00, which means 40 phr of silica and 00 phr of calcium carbonate.
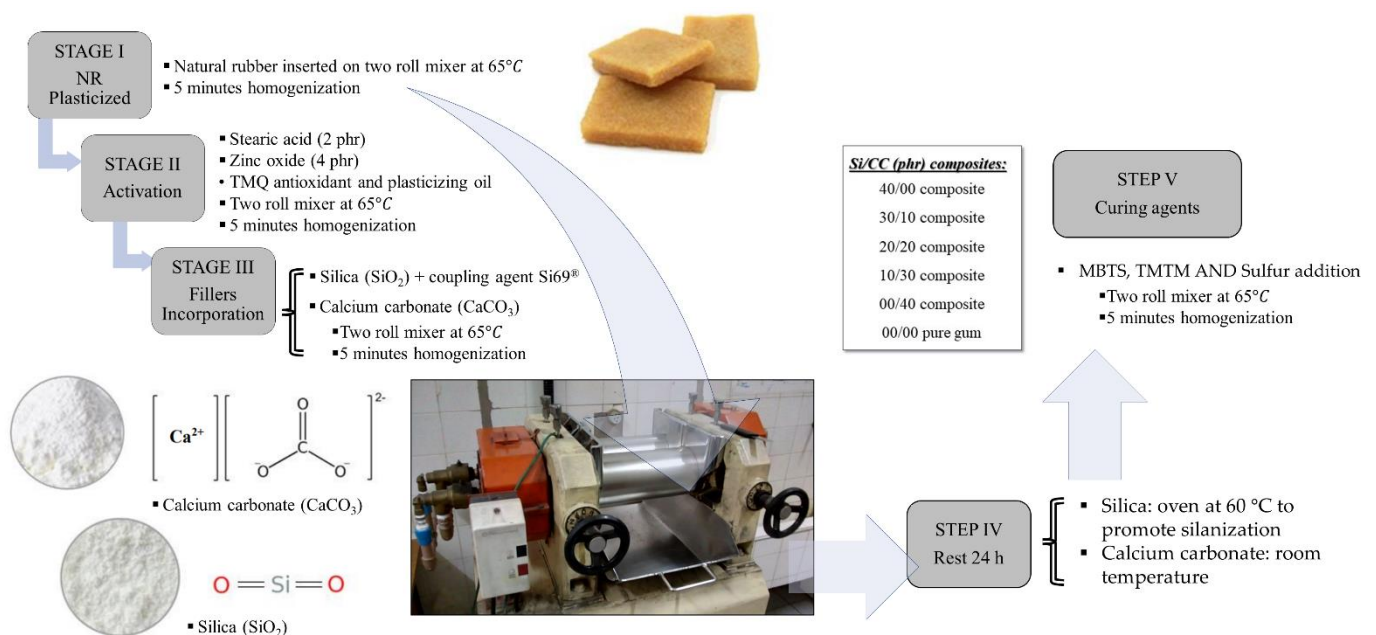

Figure 1. Natural rubber processing: from latex to vulcanization.

2.3. Measurements of Curing Characteristics

The rheometric curves were determined using a TEAM industrial rheometer 1300 W (São Bernardo do Campo, Brazil), with 1° of disk oscillation, and 150 °C isotherms, according to ASTM D2084/01 [46]. After the ideal vulcanization parameters (optimal time and temperature) were established, the material was subjected to a hot-pressing process at 150 °C using a Mastermac Vulcan 400/20-1 Press (Itapira, Brazil) with a maximum pressure of 210 kgf cm^{-2} aided by a 1010/1020 steel mold (150 mm × 150 mm × 2 mm), in accordance with ASTM D3182/0 [39].

Figure 2 presents the characteristic vulcanization curve of a sample heated to a test temperature of 150 °C. At that temperature, its viscosity decreases, which is typical of the rubber composition under testing here; this is the minimum torque point. After a while, the vulcanization starts, there is a rise of 1 or 2 dN m, and the scorch time (t_{S1}) is recorded. From this point on, the torque continues to increase until it reaches a maximum value, which occurs due to the formation of crosslinks in the polymer matrix produced by the crosslinking agent and the fillers. Considering the 90% difference between the maximum and minimum torques, the optimum vulcanization time (t_{90}) is defined. After reaching the maximum torque, reversion can occur, which means that this type of rubber cannot be over-vulcanized, or the maximum value reaches the plateaus.
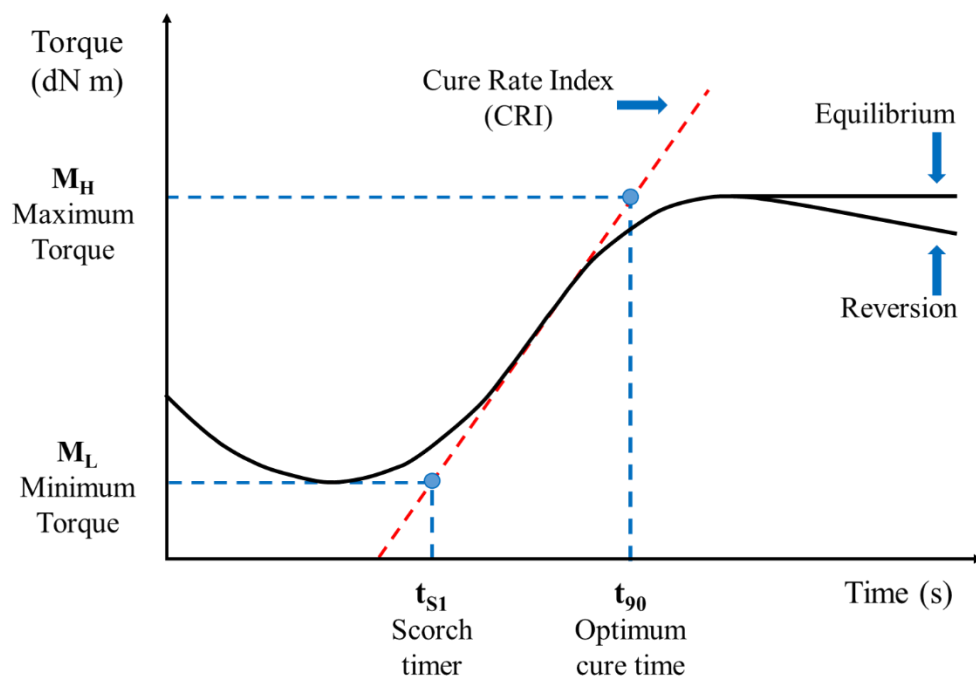

Figure 2. Rheometric curve.

2.4. Swelling Measurements

The crosslink density of the composites was determined using the swelling technique, in which samples with a mass of approximately 0.25 ± 0.05 g were weighed and immersed in toluene for 5 days. Those samples were then removed, dried up to eliminate the excess solvent, and weighed again, under environmental conditions. Then, the samples were placed in the oven at a temperature of 60 °C for 24 h and weighed once more. These values and those of dry sample mass, sample mass after swelling, and solvent mass trapped in the sample were used to calculate the VB value. Therefore, the crosslink density was calculated using Equation (1), which was developed by Flory and Rehner [47,48]:

$$\eta = \frac{-\left(\ln(1 - V_B) + V_B + \chi (V_B)^2\right)}{(\rho_B)(V_0)\left(V_B^{\frac{1}{3}} - \frac{V_B}{2}\right)} \tag{1}$$

where:

η = crosslink density (mol cm^{-3});
χ = polymer-solvent interaction parameter (or Flory parameter);
ρ_B = rubber density;
V_0 = molar volume of solvent.
V_B = rubber volume fraction in the swollen form, determined from weight gain by swelling.

The ASTM D297 standard method [49] was also used to determine the density of the composites taking into account the sample mass in air and a liquid of known density, using ethyl alcohol with a density of 0.79 g cm^{-3}. The measured masses were applied in Equation (2) [50].

$$\rho = \frac{\rho_L * m_A}{m_A - m_B} \tag{2}$$

where:

P = sample density (g/cm^{-3});
ρ_L = ethanol density at analysis temperature (g/cm^{-3});
m_A = wireless sample mass in the air (g);
m_B = wireless sample mass in liquid (g).

2.5. Measurement of Tensile Properties

The tensile tests were carried out in an electromechanical INSTRON/EMiC 23-100 (São José dos Pinhais, Brazil) universal testing machine that features a microprocessed, a strain speed of 500 mm min^{-1}, a load cell of 1000 kN, and an internal strain transducer. For this test, specimens based on ASTM D412 determinations [51], model C of samples was used, evaluating the behavior of specimens in triplicates of results. The tests were carried out in triplicate by the Department of Engineering and Architecture of the Centro Universitário Antônio Eufrásio de Toledo in Presidente Prudente, Brazil.

2.6. Measurement of Hardness (Shore A)

The influence of the incorporation of fillers into the polymeric matrix on hardness was determined according to the ASTM D2240 standard [52] using a Kiltler (São Paulo, Brazil) durometer. This method consists of forcing a penetrator on the specimen, resulting in a value that is lower the greater the depth reached.

2.7. Measurement of Abrasion-Resistance Properties

Abrasion loss was evaluated using a MaqTest (Franca, Brazil) rotating drum abrasion tester in accordance with ASTM D5963/10 standard [53], with a rotation frequency of 40 rpm, a cylinder diameter of 150 mm, and a nominal distance of 40 m. The force applied to the samples was 5.0 N at a tilt angle of 3°. The abrasion resistance index was calculated using Equation (3):

$$I_R = \frac{m_1 d_t}{m_t d_1} \times 100 \; (\%) \tag{3}$$

where:

I_R = abrasion resistance index in percentage;
m_1 = standard rubber mass (mg);
m_t = test composite mass (mg);
d_1 = standard rubber density (mg cm^{-3});
d_t = test composite density (mg cm^{-3}).

The density values of the test composites used to calculate the abrasion resistance index were the same as those presented in Table 2.

2.8. Scanning Electron Microscopy (SEM)

This study employed a Carls Zeiss EVO LS15 (Jena, Germany) scanning electron microscope using a secondary electron detector in high vacuum and constant temperature with an applied voltage of 20 kV to produce magnifications between 1000 and 10,000 times.

The samples for the SEM were prepared by fracturing the composites in their glassy state at liquid nitrogen temperature and fixed to the sample holder (stub) with double-faced carbon conductive tape. Afterward, the samples were metalized with a thin layer of gold using a Quorum Q150TE sputtering machine.

2.9. Fourier Transform Infrared (FTIR) Spectroscopy

The FTIR spectroscopy measurements were taken in a Bruker Vetor 22 (Billerica, MA, USA) spectrometer (with a wavenumber in the 500–4000 cm^{-1} range, 4 cm^{-1} of spectral resolution, and a DTGS detector using 32 scans) operating in Attenuated Total Reflectance (ATR) mode analyzed over a zinc selenide (ZnSe) window.

3. Results and Discussion

3.1. Composites with Calcium Carbonate Only

First, we studied the influence of Chartwell® as a coupling agent and compared it with silane, the coupling agent commonly used in the literature [54–59]. Figure 3 and Table 3 present the results obtained from the rheometric tests.
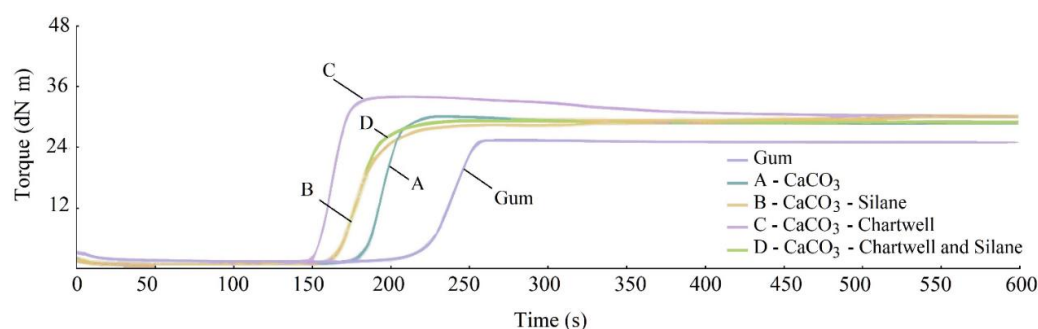

Figure 3. Rheometric curve of the NR composites with 40 phr of calcium carbonate (CaCO$_3$) measured with 1° of disk oscillation and isotherms at 150 °C. Only the coupling agents were changed. Gum is included as a reference point.

Table 3. Rheometric properties of the NR composites with 40 phr of calcium carbonate (CaCO$_3$) measured with 1° of disk oscillation and isotherms at 150 °C. Only the coupling agents were changed. Gum is included as a reference point.

Composites	t_{s1}	t_{90}	Δt	M_L	M_H	ΔM
	(s)	(s)	(s)	(dN.m)	(dN.m)	(dN.m)
Gum	192 ± 0.6	252 ± 4.7	60 ± 5	2.4 ± 0.1	26 ± 1.7	24 ± 1.8
A-CaCO$_3$ without treatment	178 ± 0.5	208 ± 0.5	30 ± 1	1.9 ± 0.1	31 ± 0.2	29 ± 0.3
B-CaCO$_3$ with silane	169 ± 7.0	213 ± 4.0	44 ± 6	1.9 ± 0.1	30 ± 1.4	28 ± 1.5
C-CaCO$_3$ with Chartwell®	148 ± 0.5	173 ± 1.5	25 ± 2	1.7 ± 0,1	35 ± 0.4	33 ± 0.5
D-CaCO$_3$ with Chartwell® and silane	161 ± 1.0	209 ± 5.0	48 ± 6	1.9 ± 0,1	31 ± 1.2	29 ± 1.3

The minimum torque, ML, is an indirect measure of the compound's viscosity. Decreasing the ML with Chartwell is related to enhanced processability, since the rheometer requires lower torque for oscillation. The enhancement in the processability by using Chartwell® as a coupling agent can be associated to improve filler dispersion and interaction between the filler and the polymer matrix [60].

The maximum torque, MH, is a characteristic of crosslinked rubber. Its value depends on the viscosity of the vulcanized product. The difference between the maximum and minimum torque, ΔM, is a parameter that defines the degree of chemical crosslinking, which reaches the maximum value for CaCO$_3$ with Chartwell® addition (33 dN.m).

Figure 4 shows the tensile strength test results of composites treated with (A) untreated 40 phr calcium carbonate, (B) silane only, (C) Chartwell® only, and (D) both. The results show an increase in tensile strength due to the synergy between the two coupling agents.
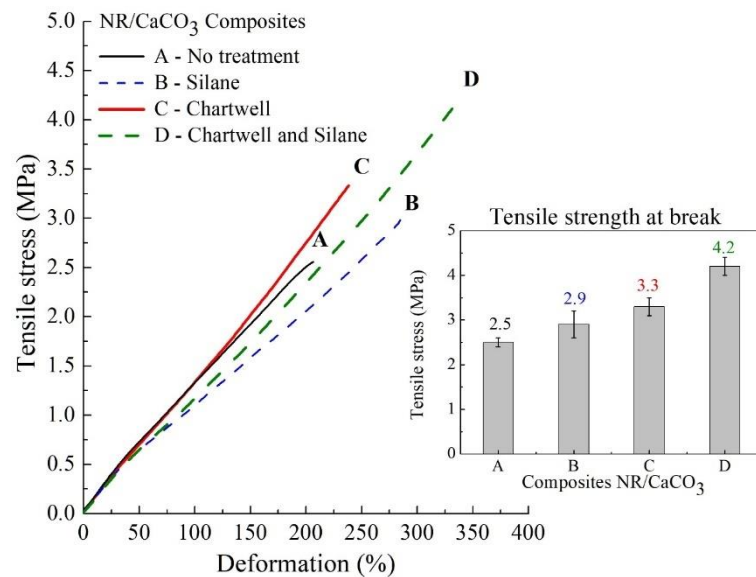

Figure 4. Tensile strength test results of the NR composites with 40 phr of calcium carbonate ($CaCO_3$) under a deformation speed of 500 mm min^{-1} and a load cell of 1000 kN. Only the coupling agents were changed.

In the (Shore A) hardness and abrasion tests (Figure 5), we observed no variation in the hardness results, but the abrasion loss of Composite D (226 mm^3/40 m) showed a decrease. This behavior is due to the synergy between the two coupling agents (silane and Chartwell®), which facilitated the dispersion and reduction of aggregates formed by the filler during their incorporation into the polymer matrix.
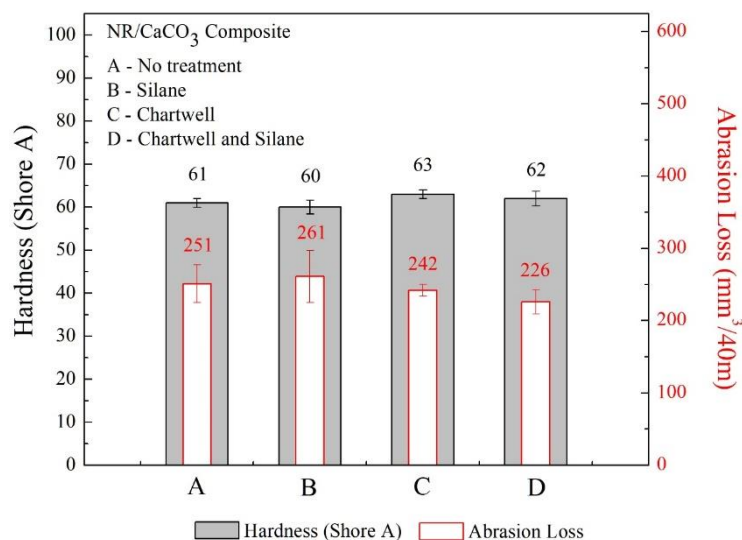

Figure 5. Shore A hardness of the NR composites with 40 phr of calcium carbonate ($CaCO_3$) measured with a Kiltler durometer and their loss of volume by abrasion measured with a rotating drum with a diameter of 150 mm at a frequency of 40 rpm and a nominal distance of 40 m. Only the coupling agents were changed.

Thus, the use of Chartwell® as a coupling agent for calcium carbonate is justified because it proved to be a viable alternative to replace or be applied in combination with

silane. Therefore, given the performance described above, calcium carbonate treated with Chartwell® was also used in this study as a partial substitute for silica in natural rubber composites, producing what we call here hybrid composites. The characteristics of these hybrid composites are presented below.

3.2. Hybrid Composites
3.2.1. Measurement of Curing Characteristics

The rheometric curves of the hybrid composites are shown in Figure 6, and their rheometric data are detailed in Table 4. The minimum and maximum torque of the composites in Table 4 present a small variation as the ratio between the fillers in the composites changes.
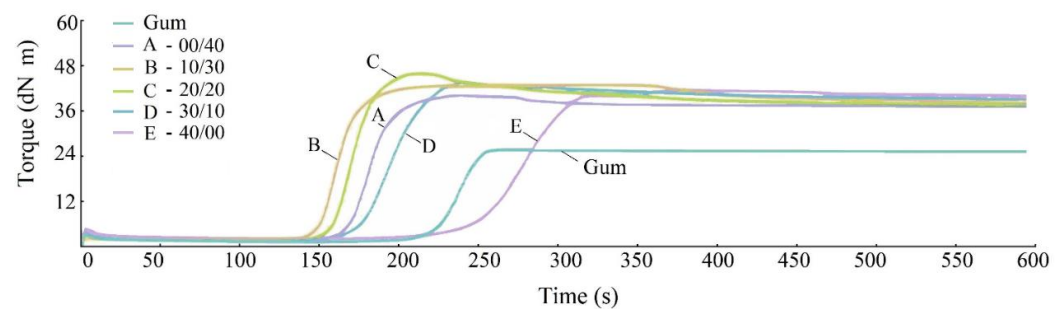

Figure 6. Rheometric curve (with 1° of disk oscillation and isotherms at 150 °C) of the hybrid composites of NR with silica (SiO_2 + Si69®) and calcium carbonate ($CaCO_3$) treated with 2% Chartwell®. Gum was included as a reference point.

Table 4. Rheometric properties (with 1° of disk oscillation and isotherms at 150 °C) of the hybrid composites of NR with silica (SiO_2 + Si69®) and calcium carbonate ($CaCO_3$) treated with 2% Chartwell®. Gum was included as a reference point.

Hybrid Composite	t_{s1}	t_{90}	Δt	M_L	M_H	ΔM
(phr)	(s)	(s)	(s)	(dN m)	(dN m)	(dN m)
Gum	212 ± 1.0	262 ± 7.2	50 ± 8.2	2.6 ± 0.2	29 ± 1.9	27 ± 2.1
00/40 (Si/CC)	158 ± 2.3	203 ± 3.2	45 ± 5.5	2.5 ± 0.1	41 ± 1.1	38 ± 1.2
10/30 (Si/CC)	146 ± 2.8	184 ± 1.4	38 ± 4.2	3.0 ± 0.1	45 ± 1.4	42 ± 1.5
20/20 (Si/CC)	150 ± 2.1	189 ± 1.4	39 ± 3.5	2.6 ± 0.4	47 ± 0.6	45 ± 1.0
30/10 (Si/CC)	162 ± 4.7	211 ± 10.6	49 ± 15.3	3.0 ± 0.2	43 ± 3.1	40 ± 3.3
40/00 (Si/CC)	224 ± 7.7	306 ± 9.3	82 ± 17.0	3.4 ± 0.2	44 ± 4.4	41 ± 4.6

Regarding the beginning of the vulcanization process, a delay was observed in the 40/00 (Si/CC in phr) composite, which is attributed to the interaction between silica and the accelerators. This behavior was also observed in its optimal healing time due to the interaction of silanol groups present on the silica surface [61]. The composites with calcium carbonate treated with Chartwell® exhibit a reduction in the interference of silica in the entire crosslinking process of the polymer matrix.

Regarding the rheometric curve of the hybrid composites (Figure 6 and Table 4), the lowest and t_{90} were achieved by Composites B and C, with 10/30 and 20/20 phr of silica and calcium carbonate, respectively. Lower t_{90} is interesting due to the faster process consequently reducing energy spend for composites preparation. However, if evaluating the linear performance after reaching the maximum torque, mainly 20/20 composites show a tendency to reversion of vulcanization observed by decreasing torque. For a conventional system of vulcanization, at the end of the vulcanization process, the excess of sulfur can cause thermal degradation of polysulfide linking, it has been observed as a reversion of curing and reduces the torque. Moreover, composites maintained a good synergy between the two coupling agents, outperforming the t_{90} of Composite E (40/00-Si/CC), which needed an optimum vulcanization time longer than five minutes. This is longer than the t_{90} of gum, which was around four and a half minutes.

The same happened with t_{s1} because the composites with treated calcium carbonate exhibited improved filler dispersion, thus decreasing their shear strength, which is reflected in the lowest values around 40 s. However, Composite E (only silica) showed the longest time. Moreover, even the decreasing scorching time (t_{s1}) and the optimal curing time (t_{90}) can reduce the able time processability, it requires us to know the desired product and properties to standard the optimum parameters. Here, the scorching time (t_{s1}) and the optimal curing time (t_{90}) decrease can be associated with the cost and spend time processing decreased, attributed to the earlier starting formation of crosslink by sulfur (t_{s1}) and the faster reach of optimum vulcanization (t_{90}). Evaluating the hybrid composites, the 30/10 Si/CC shows a lower decrease in t_{s1} compared to other amounts of Calcium Carbonate.

3.2.2. Swelling Measurements

The swelling crosslink density of the composites was determined using the Flory–Rehner equation [47,48]. As observed in Figure 7, Chartwell® is a coupling agent, leading to an increase in the crosslink density, acting similarly to the silane used as a coupling agent in a crosslinking process that employs silica as a filler [62]. The increase in the number of crosslinks was attributed to the strong physical interaction related to interfacial adhesion between the calcium carbonate particles and the polymeric chains of the matrix. The increase in the crosslink density by Calcium carbonate treated with Chartwell® can be also associated with the filler acting as a physical barrier, hindering solvent penetration, as verified by de Maria et al. [63]. However, even though these procedures occur, it is in agreement with the strong interfacial adhesion, since it did not dissociate by solvent.
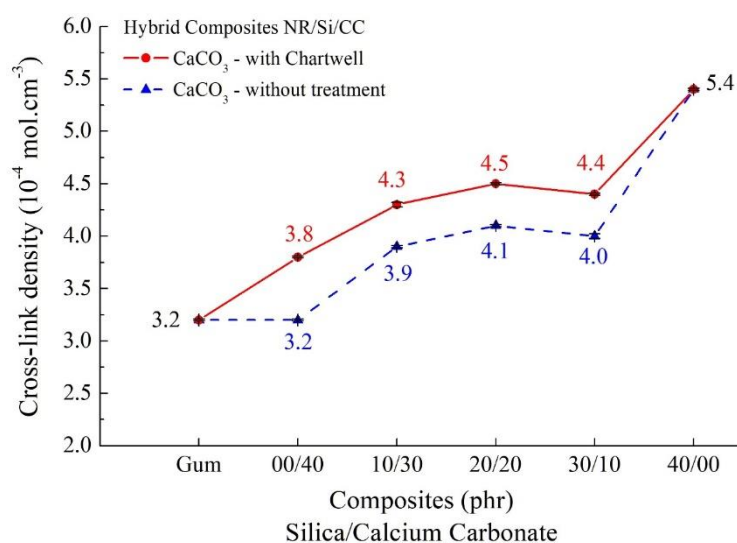

Figure 7. Crosslink density of the hybrid composites of NR with silica (SiO_2 + Si69®) and carbonate of calcium ($CaCO_3$) treated with 2% Chartwell®. Said density was calculated using the Flory–Rehner swelling equation (mass $\approx 0.25 \pm 0.05$ g, immersed in toluene for 5 days, then placed in the oven for 24 h at 60 °C). Gum was included as a reference point.

3.2.3. Measurement of Tensile Properties

Figure 8 shows the tensile stress results of the hybrid composites containing the treated calcium carbonate (which presented the best response) compared to that of their counterparts containing calcium carbonate that did not undergo surface treatment. The highest tensile stress (16.8 MPa) was obtained by the 40/00 (Si/CC in phr) which is compared to 16.7 MPa reached by the 30/10 composite in which the calcium carbonate had been treated with Chartwell® changing 10 phr of Silica. By comparison, the composite with the same proportions in which the calcium carbonate did not undergo surface treatment reached 11.3 MPa.
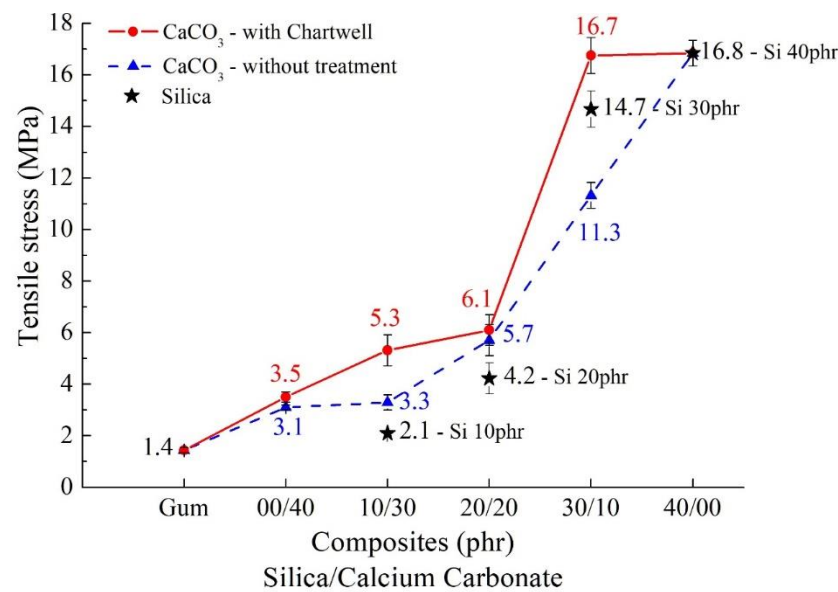
Figure 8. Tensile strength test results (at a deformation speed of 500 mm min^{-1} and a load cell of 1000 kN) of the hybrid composites of NR with silica (SiO$_2$ + Si69$^{®}$) and calcium carbonate (CaCO$_3$) treated with 2% Chartwell$^{®}$. The first composite is gum, and the silica composite (SiO$_2$ + Si69$^{®}$) was used as a reference point for comparison.

The rupture process occurs initially when the crosslinks are stressed and then broken. Only at that time, the main polymer chain breaks down. The increase in the number of crosslinks achieved using Chartwell$^{®}$ provides a higher breaking strength, which is reinforced by the polysulfide crosslinks that can rearrange under the stress associated with high tensile strength [64,65].

This 47.8% increase in tensile strength (from 11.3 to 16.7 MPa) is due to the action of the Chartwell$^{®}$ coupling agent because it promoted the anchoring of calcium carbonate fillers in the polymer matrix, restricting their mobility and increasing the tensile strength and decreasing the elongation at break (Figure 9a). Even the modulus at 100% (Figure 9b) shows similar behavior, restricting the mobility as an increased amount of Calcium Carbonate indicates the interfacial adhesion between the filler and the polymeric matrix. The crosslink density results in Figure 7 corroborating this statement.
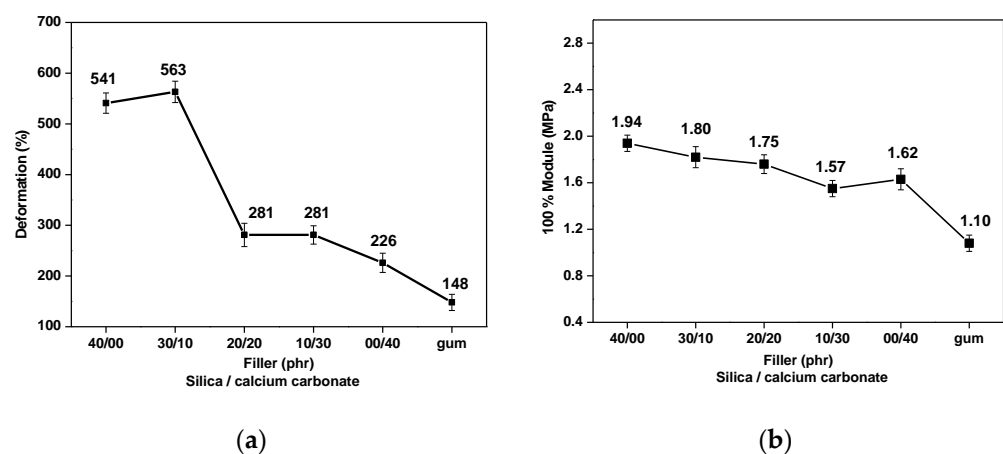

(**a**)

(**b**)

Figure 9. (**a**) Deformation at break (**b**) Modulus at 100% of hybrid composites.

3.2.4. Measurement of (Shore A) Hardness and Abrasion-Resistance Properties

Figure 10 shows the results obtained in the Shore A scale and the abrasion resistance tests. The increase in the hardness of the composites, especially that of the 30/10 (Si/CC in

phr) composite, i.e., 68 in the Shore A scale, was attributed to the presence of fillers that led to an increase in stiffness and the large number of cross-links generated by the curing agent and Chartwell® (as seen in Figure 7). Surface filler treatments contributed to restricting the mobility of the polymer chains, causing the composites to stiffen further, thus becoming more rigid than gum [66,67].
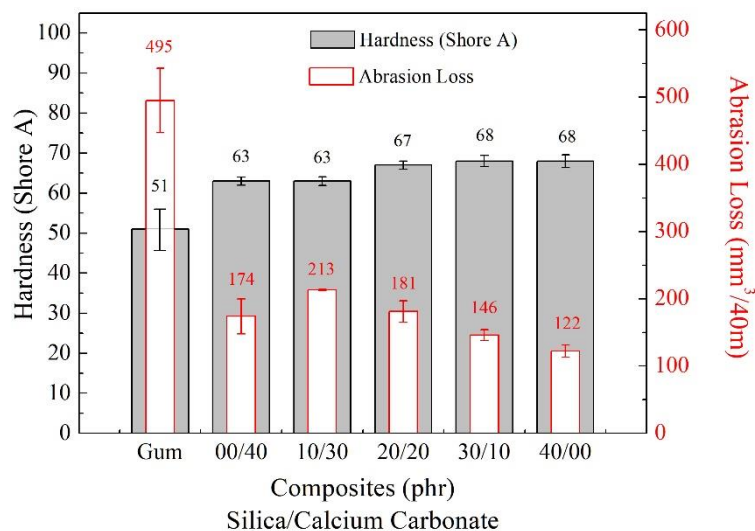

Figure 10. Shore A hardness of gum and the hybrid composites with silica (SiO_2 + Si69®) and calcium carbonate ($CaCO_3$) treated with 2% Chartwell® measured with a Kiltler durometer. The volume loss by abrasion was measured using a rotating drum, 150 mm in diameter, at a frequency of 40 rpm and a nominal distance of 40 m.

In the abrasion test, the 30/10 (Si/CC in phr) composite showed a low mass loss (146 mm^3/40 m). This behavior is attributed to the coupling agent (Chartwell®), which facilitates the dispersion of calcium carbonate and silica [68], thus preventing the formation of agglomerates and aggregates. The presence of these agglomerates and aggregates generates stress points on the composite surface, facilitating mass loss due to abrasion [69]. The composite 40/00 (Si/CC) reached the higher abrasion resistance (122 mm^3/40 m), which was not significantly changed for 30/10 composites (146 mm^3/40 m).

3.2.5. Scanning Electron Microscopy (SEM)

Figure 11 shows the SEM micrographs of the torn region on the specimens after cryogenics. It can be observed that the calcium carbonate and silica particles have a circular shape. The EDS spectrum proved that these particles are calcium carbonate (micrograph b) and silica (micrograph f), which are present throughout the samples. In addition, some voids are found on the surface of the hybrid vulcanizates with a calcium carbonate content equal to or greater than 20 phr. However, the dispersion of these fillers in the rubber matrix and the interfacial interaction between rubber and fillers were more effective in composites with a hybrid filler ratio of 30/10 due to the presence of silanol groups on the silica surface and Chartwell® on the surface of the calcium carbonate. This facilitated filler dispersion prevents the formation of agglomerates and promotes mechanical reinforcement.

3.2.6. Fourier Transform Infrared (FTIR) Spectroscopy

FTIR spectroscopy was used to study the hybrid composites with different filler ratios between silica and calcium carbonate. Figure 12 presents the main peaks found by FTIR in gum, the fillers in pure form (not incorporated), and the hybrid composites. Table 5 summarizes these results and their assignments.
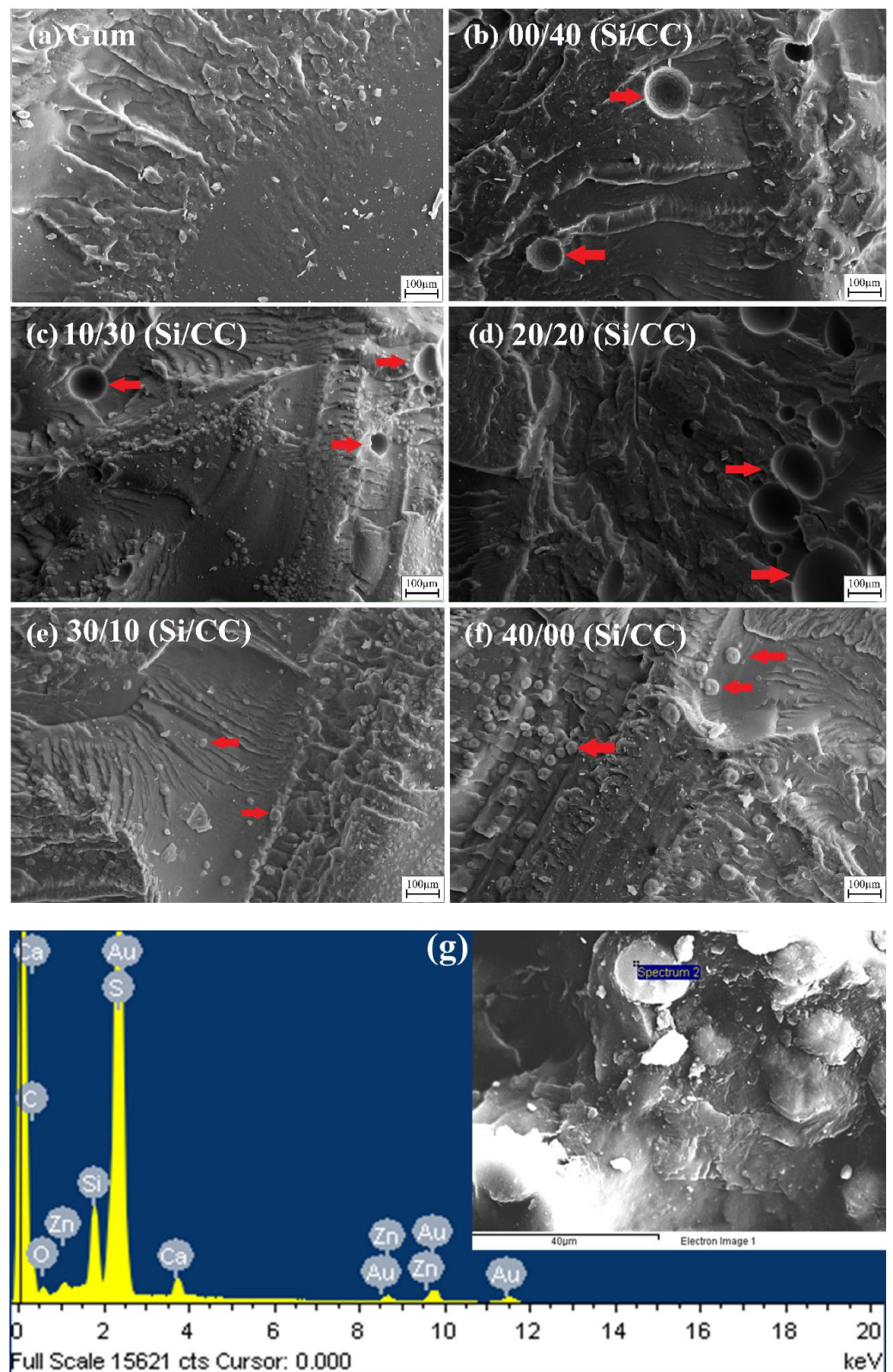
Figure 11. SEM images enlarged 200 times (cryogenically broken samples fixed with double-faced carbon conductive tape on one side and metalized with a thin layer of gold on the other side) of (**a**) gum and the NR-silica hybrid composites (SiO_2 + Si69®) with calcium carbonate ($CaCO_3$) treated with 2% Chartwell: (**b**) 00/40, (**c**) 10/30, (**d**) 20/20, (**e**) 30/10, and (**f**) 40/00. All the fractions are in phr. (**g**) EDS of the 30/10 (Si/CC in phr) composite.
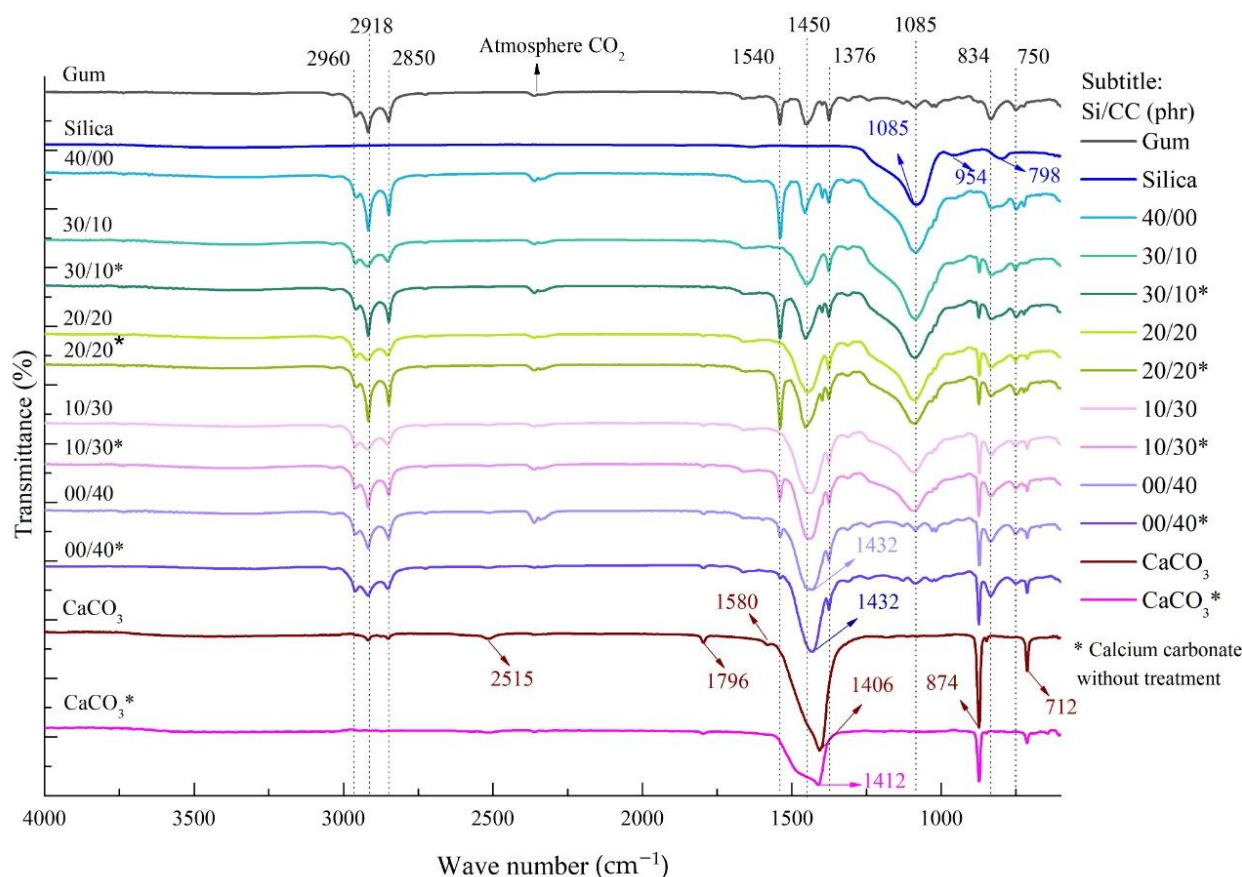
Figure 12. FTIR spectroscopy in ATR mode (4 cm^{-1} spectral resolution, DTGS detector using 32 scans, and analyzed over a zinc selenide, ZnSe, window) of the NR hybrid composites with silica (SiO$_2$ + Si69$^®$) and calcium carbonate (CaCO$_3$) treated with 2% Chartwell$^®$ and the hybrid composites with silica (SiO$_2$ + Si69$^®$) and untreated calcium carbonate (CaCO$_3$). Gum and treated and untreated fillers in pure form were included as reference points. * untreated calcium carbonate.

The peaks that correspond to the main bands of cis-1,4 polyisoprene (NR) appear at 2960 cm^{-1}, which is related to an asymmetric axial deformation of the CH bond in CH$_3$. The asymmetric and symmetric stretching of the methyl group (-CH$_3$) appears at 2918 and 2850 cm^{-1} [70,71]. The first band results from the asymmetric elongation mode, where two C-H bonds of the methyl group are extended while the third one is contracting. The second band is produced by symmetric stretching, in which all three C-H links extend and contract in phase [72].

The peak at 1540 cm^{-1}, attributed to the elongation vibration of a conjugated double bond assisted by methyl C=C (symmetric axial deformation), is more intense in untreated hybrid composites, and it practically disappears in those treated with Chartwell$^®$. This indicates that the filler surface treated with the coupling agents reacted along with the carbon-carbon, breaking the double bonds and binding to them [73,74].

In the 1450 and 1376 cm^{-1} regions, we find the asymmetric and symmetric angular deformation of the methyl group, that is, the angular deformation of CH$_2$ and the symmetric deformation of the CH$_3$ group. Finally, in the 834 cm^{-1} regions, the bending of C=CH (angular deformation) occurs in a trisubstituted olefin typical of the cis-1,4 chain [75,76], while at 750 cm^{-1} it is related to -CH$_2$ torsional vibration [77]. Thus, this set of bands and peaks characterize the polymer matrix studied here, as clearly observed in the spectrum [56,78,79].

Table 5. Main peaks of the natural rubber composite (gum) and the pure fillers (silica and calcium carbonate) found by FTIR in ATR mode (4 cm^{-1} spectral resolution, DTGS detector using 32 scans, and analyzed over a zinc selenide, ZnSe, window).

Wavenumber (cm^{-1})	Assignment	References
	Natural Rubber (cis-1,4-polyisoprene)	
2960	Asymmetric axial deformation—C-H	[59–61]
2918	Asymmetric stretch—CH$_3$	[59–61]
2850	Symmetric stretch—CH$_3$	[59–61]
1540	Symmetric axial deformation—C = C	[47,48]
1450	Asymmetric angular deformation—CH$_2$	[62–66]
1376	Symmetric angular deformation—CH$_3$	[62–66]
834	Link bending—C = CH	[62–66]
750	Twist—CH$_2$	[64]
	Silica-Silicon dioxide-SiO$_2$	
1085	Asymmetric stretch—O-Si-O	[76,77]
954	Symmetric stretch—O-Si-O	[76,77]
798	Symmetric stretch—O-Si-O	[76,77]
	Calcium carbonate-Carbon dioxide-CaCO$_3$	
1406	Amorphous phase vibration—CO$_3$	[70–73]
874	Asymmetric axial deformation—CO$_3$	[70–73]
712	Symmetric axial deformation—CO$_3$	[70–73]

Concerning calcium carbonate, two well-defined peaks were recorded in the regions around 712 cm^{-1} and 874 cm^{-1}; they are associated with the symmetric and asymmetric axial deformation of CO$_3$, respectively [80–82]. The band at 1406 cm^{-1} is attributed to a low crystalline phase of calcite (CaCO$_3$), and the band at 1796 cm^{-1} is attributed to vibrations of carbonate ions common in crystalline polymorphism [83–85]. The other bands that show less intensity compared to that of the carbonate ion [86–88] can be attributed to the capping agent.

Silica showed characteristic peaks around 1100 cm^{-1} that are attributed to the siloxane functional group. Therefore, the band of strong intensity at 1085 cm^{-1} is attributed to the asymmetric stretching vibration of the O-Si-O bond, while the bands at 954 and 798 cm^{-1} are attributed to the symmetric stretch vibration of the said bond [89,90].

Regarding the composites, the peaks at 2960 and 2850 cm^{-1} can be related to the asymmetric and symmetric stretching of CH$_2$, which validates the presence of silane on the silica surface, especially in the 40/00 (Si/CC) composite [51].

Jarnthong et al. [91] highlight that there is an elongation of amide I and flexion in the plane of amide II at 1630 cm^{-1} and 1541 cm^{-1}, respectively, which can be attributed to the inter- and intramolecular hydrogen bond between the protein molecules in the groups present in natural rubber and the silane of silica.

Likewise, Jiao et al. [92], who studied a silane-grafted ethylene-octene copolymer, reported that the peaks at 1167, 1105, 1082, and 958 cm^{-1} could be attributed to the Si-OCH$_2$CH$_3$ deformation of the silane coupling agent.

However, gum also shows the same absorption ranges between 1400 and 700 cm^{-1}; thus, it is difficult to say that there were Si–O–C deformations in the composites when silane was added. Consequently, after analyzing the results of this technique and the mechanical tests, we can affirm that signaling occurred.

In the 1432 cm^{-1} region present in the composites, mainly those with only 40 phr of CaCO$_3$, there is a band associated with the asymmetric stretching of CO$_3$ that may indicate carbonation by calcium carbonate [93].

This infrared analysis revealed significant changes in the characteristic absorption bands of the chemical structure of the composites compared to gum (polymer matrix), which were caused by the incorporation of the fillers.

The vibration of the characteristic connections present in the composites demonstrates the presence of fillers because the differences in their characteristic bands appear in intensities that vary according to the quantity of each incorporated filler. The partial replacement of silica

with calcium carbonate is evidenced in the transition of the composites from 40/00 to 00/40 (silica/calcium carbonate in phr) and reflected in the bands at 1406, 1085, and 872 cm^{-1}.

In conclusion, the fillers dispersed in the polymer matrix possibly had a chemical interaction with the latter. The Chartwell C-515.71HR® coupling agent has bifunctional molecules because they were able to connect the calcium carbonate (organic) and the polymeric matrix (inorganic), which produced peak changes due to variations in the electronegativity of neighboring atoms (such as the hydrogen bond) and the energy level of infrared light needed to cause this molecular vibration [68,94].

4. Conclusions

Physical-mechanical properties of hybrid natural rubber composites with Chartwell® coupling agent-treated calcium carbonate and silica-reinforced were evaluated. Commonly silica is the main reinforcement filler used in natural rubber products. In fact, the composites 40/00 (Si/CC) had reached higher tensile strength (16.8 MPa), hardness (68 on Shore A scale), and superior abrasion resistance. However, the cost of silica is higher than calcium carbonate, which is another commonly used rubber filler. Thus, hybrid composites have been evaluated to obtain similar mechanical properties with low cost and a faster vulcanization process when compared to rubber-based silica. Among the hybrid composites investigated here, the 30/10 (Si/CC in phr) achieved significant results as tensile strength reaching 16.7 MPa and hardness of 68 in Shore A scale comparable to composites with only silica as well as keeping a lower abrasion mass loss (146 mm^3/40 m). Therefore, Silica (SiO$_2$ + Si69®) in NR was successfully replaced with calcium carbonate (CaCO$_3$) treated with Chartwell C-515.71HR® while Chartwell C-515.71HR® successfully performed the function of coupling agent for the calcium carbonate surface treated with 2% in hybrid composites by keeping the original properties of the composites even decreasing the amount of silica. The cost of calcium carbonate treatment is 56% that of silica treated with silane, thus generating savings of approximately 11% in processing costs. Moreover, the t$_{90}$ of composites 30/10 reached 211 s, smaller as compared to 40/00 (306 s), decreasing also t$_{s1}$, which directly imply on the cost and time released over the production process, which represents an interesting financial alternative for the rubber industry.

References

1. Wipatkrut, P.; Poompradub, S. Exfoliation approach for preparing high conductive reduced graphite oxide and its application in natural rubber composites. *Mater. Sci. Eng. B* **2017**, *218*, 74–83. [CrossRef]
2. Wu, X.; Lu, C.; Han, Y.; Zhou, Z.; Yuan, G.; Zhang, X. Cellulose nanowhisker modulated 3D hierarchical conductive structure of carbon black/natural rubber nanocomposites for liquid and strain sensing application. *Compos. Sci. Technol.* **2016**, *124*, 44–51. [CrossRef]
3. Jo, J.O.; Saha, P.; Kim, N.G.; Chang Ho, C.; Kim, J.K. Development of nanocomposite with epoxidized natural rubber and functionalized multiwalled carbon nanotubes for enhanced thermal conductivity and gas barrier property. *Mater. Des.* **2015**, *83*, 777–785. [CrossRef]
4. Dick, T.A.; dos Santos, L.A. In situ synthesis and characterization of hydroxyapatite/natural rubber composites for biomedical applications. *Mater. Sci. Eng. C* **2017**, *77*, 874–882. [CrossRef]
5. Dias, F.J.; Issa JP, M.; Coutinho-Netto, J.; Fazan VP, S.; Sousa, L.G.; Iyomasa, M.M.; Watanabe, I. Morphometric and high-resolution scanning electron microscopy analysis of low-level laser therapy and latex protein (*Hevea brasiliensis*) administration following a crush injury of the sciatic nerve in rats. *J. Neurol. Sci.* **2015**, *349*, 129–137. [CrossRef] [PubMed]
6. Murniati, R.; Sutisna Wibowo, E.; Rokhmat, M.; Iskandar, F.; Abdullah, M. Natural Rubber Nanocomposite as Human-Tissue-Mimicking Materials for Replacement Cadaver in Medical Surgical Practice. *Procedia Eng.* **2017**, *170*, 101–107. [CrossRef]
7. Wisutiratanamanee, A.; Poochinda, K.; Poompradub, S. Low-temperature particle synthesis of titania/silica/natural rubber composites for antibacterial properties. *Adv. Powder Technol.* **2017**, *28*, 1263–1269. [CrossRef]
8. Ramírez-Hernández, A.; Aparicio-Saguilán, A.; Reynoso-Meza, G.; Carrillo-Ahumada, J. Multi-objective optimization of process conditions in the manufacturing of banana (*Musa paradisiaca* L.) starch/natural rubber films. *Carbohydr. Polym.* **2017**, *157*, 1125–1133. [CrossRef]
9. Al-Mansob, R.A.; Ismail, A.; Yusoff NI, M.; Albrka, S.I.; Azhari, C.H.; Karim, M.R. Rheological characteristics of unaged and aged epoxidised natural rubber modified asphalt. *Constr. Build. Mater.* **2016**, *102*, 190–199. [CrossRef]
10. Ivanoska-Dacikj, A.; Bogoeva-Gaceva, G.; Rooj, S.; Wießner, S.; Heinrich, G. Fine tuning of the dynamic mechanical properties of natural rubber/carbon nanotube nanocomposites by organically modified montmorillonite: A first step in obtaining high-performance damping material suitable for seismic application. *Appl. Clay Sci.* **2015**, *118*, 99–106. [CrossRef]
11. Muhammad, B.; Ismail, M.; Yussuf, A.A.; Muhammad, A.R.B. Elastomeric influence of natural rubber latex on cement mortar at high temperatures using thermal degradation analysis. *Constr. Build. Mater.* **2011**, *25*, 2223–2227. [CrossRef]
12. Fan, X.; Xu, H.; Zhang, Q.; Xiao, D.; Song, Y.; Zheng, Q. Insight into the weak strain overshoot of carbon black filled natural rubber. *Polymer* **2019**, *167*, 109–117. [CrossRef]
13. Hao, Z.; Lu, X.; Shen, Z.; Shen, J.; Sheng, X.; Luo, Z.; Zheng, Q. Processing rheological behavior of functionalized silica/natural rubber composites. *Mater. Res. Express* **2019**, *6*, 085303. [CrossRef]
14. Khouchaf, L.; Oufakir, A. Fabrication, Design and Characterization of 1D Nano-Fibrous SiO2 Surface by a Facile and Scalable Method. *Crystals* **2022**, *12*, 531. [CrossRef]
15. Amin, N.; Gul, S.; Sultana, S.; Alam, S. Preparation and Characterization of Mesoporous Silica from Bagasse Bottom Ash from the Sugar Industry. *Crystals* **2021**, *11*, 938. [CrossRef]
16. Tran, H.-B.; Le, V.-B.; Phan, V.T.-A. Mechanical Properties of High Strength Concrete Containing Nano SiO2 Made from Rice Husk Ash in Southern Vietnam. *Crystals* **2021**, *11*, 932. [CrossRef]
17. Alotaibi, M.S.; Almousa, N.H.; Asaker, M.A.; Alkasmoul, F.S.; Khdary, N.H.; Khayyat, M. Morphological: Optical, and Mechanical Characterizations of Non-Activated and Activated Nanocomposites of SG and MWCNTs. *Crystals* **2021**, *11*, 1280. [CrossRef]
18. Lee, C.-W.; Hwang, T.; Nam, G.-Y.; Hong, J.-P.; Lee, D.-A.; Oh, J.-S.; Kwak, S.B.; Lee, S.-H.; Lee, W.-S.; Yang, K.-M.; et al. A novel synthetic route to natural rubber/montmorillonite nanocomposites using colloid stabilization–destabilization method. *Compos. Part A Appl. Sci. Manuf.* **2011**, *42*, 1826–1832. [CrossRef]
19. Rooj, S.; Das, A.; Thakur, V.; Mahaling, R.N.; Bhowmick, A.K.; Heinrich, G. Preparation and properties of natural nanocomposites based on natural rubber and naturally occurring halloysite nanotubes. *Mater. Des.* **2010**, *31*, 2151–2156. [CrossRef]
20. Kang, H.; Tang, Y.; Yao, L.; Yang, F.; Fang, Q.; Hui, D. Fabrication of graphene/natural rubber nanocomposites with high dynamic properties through convenient mechanical mixing. *Compos. Part B Eng.* **2017**, *112*, 1–7. [CrossRef]
21. Jacob, M.; Thomas, S.; Varughese, K.T. Mechanical properties of sisal/oil palm hybrid fiber reinforced natural rubber composites. *Compos. Sci. Technol.* **2004**, *64*, 955–965. [CrossRef]
22. Pantamanatsopa, P.; Ariyawiriyanan, W.; Meekeaw, T.; Suthamyong, R.; Arrub, K.; Hamada, H. Effect of Modified Jute Fiber on Mechanical Properties of Green Rubber Composite. *Energy Procedia* **2014**, *56*, 641–647. [CrossRef]
23. Geethamma, V.G.; Kalaprasad, G.; Groeninckx, G.; Thomas, S. Dynamic mechanical behavior of short coir fiber reinforced natural rubber composites. *Compos. Part A Appl. Sci. Manuf.* **2005**, *36*, 1499–1506. [CrossRef]
24. Zhou, Y.; Ge, L.; Fan, N.; Dai, L.; Xia, M. Cure characteristics, mechanical, thermal, and coloring properties of natural rubber/dye-loaded shell powder composites. *J. Appl. Polym. Sci.* **2017**, *135*, 45750. [CrossRef]
25. Dos Santos, R.J.; Agostini, D.L.D.S.; Cabrera, F.C.; Dos Reis, E.A.P.; Ruiz, M.R.; Budemberg, E.R.; Teixeira, S.R.; Job, A.E. Sugarcane bagasse ash: New filler to natural rubber composite. *Polímeros* **2014**, *24*, 646–653. [CrossRef]
26. Xie, T.; Wang, F.; Xie, C.; Lei, S.; Yu, S.; Liu, J.; Huang, D. Mechanical Properties of Natural Rubber Filled with Foundry Waste Derived Fillers. *Materials* **2019**, *12*, 1863. [CrossRef]

27. Garcia, N.G.; dos Reis, E.A.P.; Budemberg, E.R.; Agostini, D.L.S.; Salmazo, L.O.; Cabrera, F.C.; Job, A.E. Natural rubber/leather waste composite foam: A new eco-friendly material and recycling approach. *J. Appl. Polym. Sci.* **2014**, *132*, 41636. [CrossRef]

28. Santos, R.J.; Agostini DL, S.; Cabrera, F.C.; Budemberg, E.R.; Job, A.E. Recycling leather waste: Preparing and studying on the microstructure, mechanical, and rheological properties of leather waste/rubber composite. *Polym. Compos.* **2014**, *36*, 2275–2281. [CrossRef]

29. Pittayavinai, P.; Thanawan, S.; Amornsakchai, T. Manipulation of mechanical properties of short pineapple leaf fiber reinforced natural rubber composites through variations in cross-link density and carbon black loading. *Polym. Test.* **2016**, *54*, 84–89. [CrossRef]

30. Ismail, H.; Edyham, M.R.; Wirjosentono, B. Bamboo fibre filled natural rubber composites: The effects of filler loading and bonding agent. *Polym. Test.* **2002**, *21*, 139–144. [CrossRef]

31. Lai, S.-M.; Guo, G.-L.; Han, K.-T.; Huang, P.-S.; Huang, Z.-L.; Jiang, M.-J.; Zou, Y.-R. Properties and characterization of near infrared-triggered natural rubber (NR)/carnauba wax (CW)/carbon nanotube (CNT) shape memory bio-nanocomposites. *J. Polym. Res.* **2019**, *26*, 86. [CrossRef]

32. George, N.; Venugopal, B.; John, H.; Mathiazhagan, A.; Joseph, R. Nanosilica decorated multiwalled carbon nanotubes (CS hybrids) in natural rubber latex. *Polymer* **2018**, *161*, 170–180. [CrossRef]

33. Kim, W.S.; Paik, H.J.; Bae, J.-W.; Kim, W. Effect of polyethylene glycol on the properties of styrene-butadiene rubber/organoclay nanocomposites filled with silica and carbon black. *J. Appl. Polym. Sci.* **2011**, *122*, 1766–1777. [CrossRef]

34. Jong, L. Synergistic effect of calcium carbonate and biobased particles for rubber reinforcement and comparison to silica reinforced rubber. *J. Compos. Sci.* **2020**, *4*, 113. [CrossRef]

35. Phuhiangpa, N.; Ponloa, W.; Phongphanphanee, S.; Smitthipong, W. Performance of nano-and microcalcium carbonate in uncrosslinked natural rubber composites: New results of structure–properties relationship. *Polymers* **2020**, *12*, 2002. [CrossRef]

36. Phuhiangpa, N.; Phongphanphanee, S.; Smitthipong, W. Study of rubber/calcium carbonate composites. In: IOP Conference Series: Materials Science and Engineering. *IOP Publ.* **2020**, *773*, 012013. [CrossRef]

37. Prasertsri, S.; Vudjung, C.; Inthisaeng, W.; Srichan, S.; Sapprasert, K.; Kongon, J. Comparison of reinforcing efficiency between calcium carbonate/carbon black and calcium carbonate/silica hybrid filled natural rubber composites. In *Defect and Diffusion Forum*; Trans Tech Publications Ltd.: Bäch, Switzerland, 2018; pp. 94–98. [CrossRef]

38. Mogy, E.; Soma, A.; Darwish, N.A.; Awad, A. Comparative study of the cure characteristics and mechanical properties of natural rubber filled with different calcium carbonate resources. *J. Vinyl Addit. Technol.* **2020**, *26*, 309–315. [CrossRef]

39. Tangboriboon, N.; Takkire, R.; Sangwan, W.; Changkhamchom, S.; Sirivat, A. Bio-CaCO3 from raw eggshell as additive in natural rubber latex glove films. Rubber. *Chem. Technol.* **2019**, *92*, 558–577. [CrossRef]

40. Sun, Q.Y.; Sun, C. Dosage Determination of Aluminate Coupling Agent Modifying Nano-Calcium Carbonate. *Adv. Mater. Res.* **2011**, *347*, 214–217. [CrossRef]

41. Doufnoune, R.; Haddaoui, N.; Riahi, F. The Interactions of Silane and Zirconate Coupling Agents with Calcium Carbonate. *Int. J. Polym. Mater. Polym. Biomater.* **2007**, *56*, 227–246. [CrossRef]

42. Sampath, W.; Egodage, S.; Edirisinghe, D. Effect of an organotitanate coupling agent on properties of calcium carbonate filled low-density polyethylene and natural rubber composites. *J. Natl. Sci. Found. Sri Lanka* **2019**, *47*, 17–27. [CrossRef]

43. Yang, Z.; Tang, Y.; Zhang, J. Surface modification of CaCO$_3$ nanoparticle with silane coupling agent for improvement of interfacial compatibility with styrene-butadiene rubber (SBR). *Chalcogenide Lett.* **2013**, *10*, 131–141.

44. Chartwell International. Technical data Chartwell C-515.71HR. Available online: http://chartwellintl.com (accessed on 10 October 2017).

45. *ASTMD3182*; Standard Practice for Rubber—Materials, Equipment, and Procedures for Mixing Standard Compounds and Preparing Standard Vulcanized. ASTM—American Society for Testing and Materials: West Conshohocken, PA, USA, 2013; pp. 1–3.

46. *ASTM D2084*; Standard Test Method for Rubber Property-Vulcanization Using Oscillating Disk Cure Meter. ASTM—American Society for Testing and Materials: West Conshohocken, PA, USA, 2001; pp. 1–12.

47. Vieyres, A.; Pérez-Aparicio, R.; Albouy, P.-A.; Sanseau, O.; Saalwächter, K.; Long, D.R.; Sotta, P. Sulfur-Cured Natural Rubber Elastomer Networks: Correlating Cross-Link Density, Chain Orientation, and Mechanical Response by Combined Techniques. *Macromolecules* **2013**, *46*, 889–899. [CrossRef]

48. Flory, P.J.; Rehner, J., Jr. Statistical Mechanics of Cross-Linked Polymer Networks II. Swelling. *J. Chem. Phys.* **1943**, *11*, 521. [CrossRef]

49. *ASTM D792*; Standard Test Methods for Density and Specific Gravity (Relative Density) of Plastics. ASTM—American Society for Testing and Materials: West Conshohocken, PA, USA, 2014; pp. 1–6.

50. *ASTM D297*; Test Method for Rubber Property—Chemical Analysis. ASTM—American Society for Testing and Materials: West Conshohocken, PA, USA, 1986.

51. *ASTM D412*; Test Methods for Vulcanized Rubber and Thermoplastic Elastomers—Tension. ASTM—American Society for Testing and Materials: West Conshohocken, PA, USA, 2013.

52. *ASTM D2240*; Test Method for Rubber Property—Durometer Hardness. ASTM—American Society for Testing and Materials: West Conshohocken, PA, USA, 2010.

53. *ASTM D5963*; Test Method for Rubber Property—Abrasion Resistance (Rotary Drum Abrader). ASTM—American Society for Testing and Materials: West Conshohocken, PA, USA, 2010.

54. Xiao, Y.; Zou, H.; Zhang, L.; Ye, X.; Han, D. Surface modification of silica nanoparticles by a polyoxyethylene sorbitan and silane coupling agent to prepare high-performance rubber composites. *Polym. Test.* **2020**, *81*, 106195. [CrossRef]

55. Radabutra, S.; Khemthong, P.; Saengsuwan, S. Effect of silane coupling agent pretreatment on the properties of rice straw particleboard bonded with prevulcanized natural rubber latex. *J. Rubber Res.* **2021**, *24*, 157–163. [CrossRef]

56. Han, S.; Gu, B.; Kim, S.; Kim, S.; Mun, D.; Morita, K.; Kim, D.; Kim, W. Effect of Sulfur Variation on the Vulcanizate Structure of Silica-Filled Styrene-Butadiene Rubber Compounds with a Sulfide–Silane Coupling Agent. *Polymers* **2020**, *12*, 2815. [CrossRef] [PubMed]

57. Ye, N.; Zheng, J.; Ye, X.; Xue, J.; Han, D.; Xu, H.; Wang, Z.; Zhang, L. Performance enhancement of rubber composites using VOC-Free interfacial silica coupling agent. *Compos. Part B Eng.* **2020**, *202*, 108301. [CrossRef]

58. Lee, S.Y.; Kim, J.S.; Lim, S.H.; Jang, S.H.; Kim, D.H.; Park, N.-H.; Jung, J.W.; Choi, J. The investigation of the silica-reinforced rubber polymers with the methoxy type silane coupling agents. *Polymers* **2020**, *12*, 3058. [CrossRef]

59. Kaewsikoun, S.; Kumarn, S.; Sakdapipanich, J. The effect of non-rubber components on mechanical properties of TESPD silane coupling agent in silica-filled rubber compounds. In Proceedings of the IOP Conference Series: Materials Science and Engineering, Ulaanbaatar, Mongolia, 10–13 September 2020; IOP Publishing: Bristol, UK, 2020; Volume 773. No. 1. [CrossRef]

60. Mottaghi, M.; Khorasani, S.N.; Esfahany, M.N.; Farzadfar, A.; Talakesh, M. Comparison of the effect of nano ZnO and conventional grade ZnO on the cross-linking densities of NR/BR and NR/SBR blends. *J. Elastomers Plast.* **2012**, *44*, 443–451. [CrossRef]

61. Boonmee, A.; Jarukumjorn, K. Preparation and characterization of silica nanoparticles from sugarcane bagasse ash for using as a filler in natural rubber composites. *Polym. Bull.* **2020**, *77*, 3457–3472. [CrossRef]

62. Sattayanurak, S.; Noordermeer, J.W.; Sahakaro, K.; Kaewsakul, W.; Dierkes, W.K.; Blume, A. Silica-reinforced natural rubber: Synergistic effects by addition of small amounts of secondary fillers to silica-reinforced natural rubber tire tread compounds. *Adv. Mater. Sci. Eng.* **2019**, *2019*, 5891051. [CrossRef]

63. de Maria, V.P.K.; de Paiva, F.F.G.; Cabrera, F.C.; Hiranobe, C.T.; Ribeiro, G.D.; Paim, L.L.; dos Santos, R.J. Mechanical and rheological properties of partial replacement of carbon black by treated ultrafine calcium carbonate in natural rubber compounds. *Polym. Bull.* **2021**, *79*, 7969–7987. [CrossRef]

64. Idrus, S.S.; Ismail, H.; Palaniandy, S. Study of the effect of different shapes of ultrafine silica as fillers in natural rubber compounds. *Polym. Test.* **2011**, *30*, 251–259. [CrossRef]

65. Oliveira, M.A.D.S.; Cassu, S.N.; De Mello, S.A.C.; Dutra, J.C.N. Influência do método de vulcanização nas propriedades mecânicas e na densidade de ligações cruzadas da borracha natural. *Polímeros* **2016**, *26*, 43–48. [CrossRef]

66. Rao, S.; Devi SN, S.; Johns, A.; Kalkornsurapranee, E.; Sham Aan, M.; Johns, J. Mechanical and thermal properties of carbon black reinforced natural rubber/polyvinyl alcohol fully interpenetrating polymer networks. *J. Vinyl Addit. Technol.* **2016**, *24*, 21–29. [CrossRef]

67. Hundiwale, D.G.; Kapadi, U.R.; Desai, M.C.; Bidkar, S.H. Mechanical properties of natural rubber filled with flyash. *J. Appl. Polym. Sci.* **2002**, *85*, 995–1001. [CrossRef]

68. Xu, T.; Jia, Z.; Wang, S.; Chen, Y.; Luo, Y.; Jia, D.; Peng, Z. Self-crosslinkable epoxidized natural rubber-silica hybrids. *J. Appl. Polym. Sci.* **2016**, *134*. [CrossRef]

69. De, S.K.; White, J.R. (Eds.) *Rubber Technologist's Handbook*; iSmithers Rapra Publishing: Online, 2001; pp. 159, 330, 356.

70. Rúvulo Filho, A. Físico-Químico de Filmes de Borracha Clorada. Ph.D. Thesis, Instituto de Física e Química de São Carlos, Universidade de São Paulo, São Carlos, Brasil, 1986.

71. Marinho, J.R.D. Microestrutura de Cis-Poliisopreno de Látices Naturais. Ph.D. Thesis, Instituto de Macromoléculas, Universidade Federal do Rio de Janeiro, Rio de Janeiro, Brasil, 1992.

72. Gunasekaran, S.; Natarajan, R.K.; Kala, A. FTIR spectra and mechanical strength analysis of some selected rubber derivatives. *Spectrochim. Acta Part A Mol. Biomol. Spectrosc.* **2007**, *68*, 323–330. [CrossRef]

73. Coleman, M.M.; Shelton, J.R.; Koenig, J.L. Raman Spectroscopic Studies of the Vulcanization of Rubbers. III. Studies of Vulcanization Systems Based on 2-Mercaptobenzothiazole. *Rubber Chem. Technol.* **1972**, *45*, 173–181. [CrossRef]

74. Koenig, J.L.; Coleman, M.M.; Shelton, J.R.; Starmer, P.H. Raman Spectrographic Studies of the Vulcanization of Rubbers. I. Raman Spectra of Vulcanized Rubbers. *Rubber Chem. Technol.* **1971**, *44*, 71–86. [CrossRef]

75. Dall'Antonia, A.C.; Martins, M.A.; Moreno RM, B.; Mattoso LH, C.; Gonçalves, P.S.; Job, A.E. Caracterização mecânica e térmica da borracha natural formulada e vulcanizada dos clones: GT 1, IAN 873, PB 235 e RRIM 600. *Polímeros* **2009**, *19*, 63–71. [CrossRef]

76. Visconte, L.L.Y.; Martins, A.F.; Nunes, R.C.R.; Suarez, J.C.M. NR/SBR Blends: Preparation Modes and Properties. *Polímeros* **2001**, *11*, 76–81. [CrossRef]

77. Barboza-Filho, C.G.; Cabrera, F.C.; Dos Santos, R.J.; De Saja Saez, J.A.; Job, A.E. The influence of natural rubber/Au nanoparticle membranes on the physiology of Leishmania brasiliensis. *Exp. Parasitol.* **2012**, *130*, 152–158. [CrossRef] [PubMed]

78. Vahabi, A.; Ramezanianpour, A.A.; Sharafi, H.; Zahiri, H.S.; Vali, H.; Noghabi, K.A. Calcium carbonate precipitation by strainBacillus licheniformisAK01, newly isolated from loamy soil: A promising alternative for sealing cement-based materials. *J. Basic Microbiol.* **2013**, *55*, 105–111. [CrossRef] [PubMed]

79. Panrat, K.; Boonme, P.; Taweepreda, W.; Pichayakorn, W. Formulations of Natural Rubber Latex as Film Former for Pharmaceutical Coating. *Procedia Chem.* **2012**, *4*, 322–327. [CrossRef]

80. Gunasekaran, S.; Anbalagan, G.; Pandi, S. Raman and infrared spectra of carbonates of calcite structure. *J. Raman Spectrosc.* **2006**, *37*, 892–899. [CrossRef]

81. Reig, F.B.; Adelantado, J.V.G.; Moreno, M.C.M.M. FTIR quantitative analysis of calcium carbonate (calcite) and silica (quartz) mixtures using the constant ratio method. Application to geological samples. *Talanta* **2002**, *58*, 811–821. [CrossRef]
82. White, W.B. *The Infrared Spectra of Minerals*; Farmer, V.C., Ed.; Mineralogical Society of Great Britain and Ireland: London, UK, 1974.
83. Martins, F.M. Caracterização Química e Mineralógica de Resíduos Sólidos Industriais Minerais do Estado do Paraná. Master's Thesis, Programa de pós-graduação em Química. Universidade Federal do Paraná, Curitiba, Brasil, 2006.
84. Paiva, L.B.; Morales, A.R.; Díaz, F.R.E. Organophilic clays: Characteristics, preparation methods, intercalation compounds and characterization techniques. *Cerâmica* **2008**, *54*, 213–226. [CrossRef]
85. Rodriguez-Blanco, J.D.; Shaw, S.; Benning, L.G. The kinetics and mechanisms of amorphous calcium carbonate (ACC) crystallization to calcite, viavaterite. *Nanoscale* **2011**, *3*, 265–271. [CrossRef]
86. Matei, C.; Berger, D.; Dumbrava, A.; Radu, M.D.; Gheorghe, E. Calcium carbonate as silver carrier in composite materials obtained in green seaweed extract with topical applications. *J. Sol-Gel Sci. Technol.* **2019**, *92*, 1–9. [CrossRef]
87. Wang, C.; Piao, C.; Zhai, X.; Hickman, F.N.; Li, J. Synthesis and characterization of hydrophobic calcium carbonate particles via a dodecanoic acid inducing process. *Powder Technol.* **2010**, *198*, 131–134. [CrossRef]
88. Marić-Stojanović, M.; Bajuk-Bogdanović, D.; Uskoković-Marković, S.; Holclajtner-Antunović, I. Spectroscopic analysis of XIV century wall paintings from Patriarchate of Peć Monastery, Serbia. *Spectrochim. Acta Part A Mol. Biomol. Spectrosc.* **2018**, *191*, 469–477. [CrossRef] [PubMed]
89. Araújo, L.C.P. Eletrossíntese de nanopartículas de prata em sílica como agente antimicrobiano em composições de borracha de silicone. Master's Thesis, Universidade Federal de Itajubá, Minas Gerais, Brasil, 2017.
90. Bayat, H.; Fasihi, M. Effect of coupling agent on the morphological characteristics of natural rubber/silica composites foams. *e-Polymers* **2019**, *19*, 430–436. [CrossRef]
91. Jarnthong, M.; Liao, L.; Zhang, F.; Wang, Y.; Li, P.; Peng, Z.; Malawet, C.; Intharapat, P. Characterization of interaction between natural rubber and silica by FTIR. *AIP Conf. Proc.* **2017**, *1846*, 20014. [CrossRef]
92. Jiao, C.; Wang, Z.; Gui, Z.; Hu, Y. Silane grafting and crosslinking of ethylene–octene copolymer. *Eur. Polym. J.* **2005**, *41*, 1204–1211. [CrossRef]
93. Puligilla, S.; Mondal, P. Co-existence of aluminosilicate and calcium silicate gel characterized through selective dissolution and FTIR spectral subtraction. *Cem. Concr. Res.* **2015**, *70*, 39–49. [CrossRef]
94. Munajad, A.; Subroto, C.; Suwarno. Fourier Transform Infrared (FTIR) Spectroscopy Analysis of Transformer Paper in Mineral Oil-Paper Composite Insulation under Accelerated Thermal Aging. *Energies* **2018**, *11*, 364. [CrossRef]